Investigation of the adsorption behaviour of acetone at the surface of ice. A grand canonical Monte Carlo simulation study

György Hantal, Pál Jedlovszky, Paul N.M. Hoang, Sylvain Picaud

Investigation of the adsorption behaviour of acetone at the surface of ice. A grand canonical Monte Carlo simulation study

György Hantal,*[ab] Pál Jedlovszky,[ac] Paul N. M. Hoang[b] and Sylvain Picaud[b]

The adsorption isotherm of acetone at the surface of I_h ice has been determined by a set of grand canonical Monte Carlo simulations at 200 K, by varying the chemical potential of acetone in the simulations. The obtained isotherm can be described by the Langmuir theory up to a certain relative pressure value (*i.e.*, about 0.07); above which the isotherm increasingly deviates from the Langmuir form. This deviation mainly originates from the increasing importance of the lateral dipolar interactions. Further, above this pressure the adsorption sites are no longer equivalent: the adsorbed acetone molecules are aligned in three different ways. In one of these orientations the acetone molecule forms two, while in another one it forms one hydrogen bond with the surface waters, whereas in the third preferred orientation no hydrogen bonding occurs between the adsorbed molecule and the ice surface.

1. Introduction

The interaction of atmospheric trace gases, mainly small, partially oxidized hydrocarbons (POHs), such as methanol, formaldehyde, formic acid and acetone with the surface of ice having become a subject of intensive experimental and theoretical investigations in the recent years.[1–9] This growing interest can be related to the role that trace gases play in the chemistry of the atmosphere. Indeed, the photo-oxidation of these trace gases can provide a substantial source of HO_x radicals that are responsible for driving photochemical cycles involving ozone production and loss in the upper troposphere. The upper troposphere, being at the altitude of about 8–12 km, is characterized by low temperature (188–228 K) and by the frequent presence of cirrus clouds consisting of small ice particles. These ice particles may influence the partitioning of POHs between the gaseous and solid phases, and can provide heterogeneous surfaces for their photo-degradation.

In the upper troposphere where temperatures are consistently lower than −33 °C, nucleation of ice particles mainly proceeds from a stochastic event in aqueous droplets, without catalysis from a foreign substance.[10] This process, called "homogeneous nucleation of ice", is generally assumed to produce hexagonal ice.[11] However, there are also some reports that the metastable cubic crystalline phase of ice may also form in the Earth's atmosphere, in particular, in the stratosphere.[12] For instance, about 25% of the ice crystals in Antarctic polar stratospheric clouds exhibit cubic morphology.[13]

[a] *Laboratory of Interfaces and Nanosize Systems, Institute of Chemistry, Eötvös Loránd University, Pázmány Péter stny. 1/a, H-1117 Budapest, Hungary. E-mail: hantal@elte.hu*
[b] *Institut UTINAM—UMR CNRS 6213, Faculté des Sciences, Université de Franche-Comté, F-25030 Besançon Cedex, France*
[c] *HAS Research Group of Technical Analytical Chemistry, Szt. Gellért tér 4, H-1111 Budapest, Hungary*

Among the various POHs acetone is certainly one of the most abundant molecules in the atmosphere. Singh *et al.*[14] and Jacob *et al.*[15] published data about the global sources of acetone, estimated to be about 6–8 × 10^{10} kg $year^{-1}$, 50% of which resulting from biogenic sources (*e.g.* pastures, rural forested areas), and another 50% from the atmospheric oxidation of isoalkenes (mainly propane) and monoterpenes. Moreover, recent observations have shown that, besides the above two sources, acetone can also be emitted by the polar snow packs.[16] Measurements performed later at Alert (82.5°N, 62.3°W) during the ALERT 2000 field camping[17] also demonstrated that there is an acetone exchange between the snow pack and the atmosphere, and pointed out that photochemical processes could contribute to acetone emission by the snow pack in springtime. The lifetime of the acetone molecules in the atmosphere was estimated by considering the wet and dry deposition, leading to an average of 15 days. During such a long time acetone can be transported far away in the atmosphere, even up to the upper troposphere.[18] Therefore, careful investigation of the interaction of acetone with the ice surface may reveal new processes that would need to be included in the chemistry models of the upper troposphere.

In order to characterize the influence of various organic functional groups (*e.g.*, C═O, OH, C(O)OH, C(O)H) on the interaction between POHs and ice, several experimental studies were carried out. Thus, the adsorption of acetone,[9,17–24] acetic acid,[25,26] formaldehyde,[23] formic acid,[26,27] methanol,[19,23,28] acetaldehyde,[19] and 2,3-butanedione[20] on ice has been studied using either a Knudsen cell flow reactor or a coated-wall flow tube. This work led to the conclusion that the interaction between POHs and ice is of the simplest type, *i.e.*, reversible physisorption, and the corresponding adsorption enthalpies are between −70 and −50 kJ mol^{-1}, with the exception of formaldehyde, which exhibits very low affinity to the ice surface.[23]

Although these experiments can describe the most important properties of the adsorption, they cannot answer

questions concerning several details of this process, such as how trace gases interact with the ice phase, what their preferred positions and orientations at the surface are, and whether there is a competition between the interaction with the ice phase and with the neighbouring adsorbate molecules. However, in adequately addressing these questions computer simulation methods[29] are particularly suitable, since they can provide three-dimensional samples of the system investigated at atomistic resolution. On the other hand, simulation results always have to be validated by comparisons with existing experimental data. Therefore, in a couple of previous papers we used molecular dynamics (MD) and grand canonical Monte Carlo (GCMC)[29] simulations to study the adsorption of methanol,[28,30] formaldehyde,[30,31] formic acid,[27] ethanol,[32] acetic acid,[33] and acetone[34] on ice. Indeed, these atomistic simulations allowed an accurate modelling of the POH–ice interactions by taking a sufficiently large number of molecules into account in the calculations. While the MD method is a convenient tool to determine the dynamic properties, such as the surface and bulk diffusion coefficients,[35] the GCMC method proved to be particularly suitable to determine the full adsorption isotherm. In these calculations the chemical potential of the adsorbed species is systematically varied, while the temperature and volume of the system are kept constant, and the surface density of the adsorbed molecules is calculated at each chemical potential value. The GCMC method has been successfully applied to simulate adsorption on various substrates, such as carbonaceous materials,[36–43] silica[44,45] or MgO.[46] Very recently, we used this method to study the adsorption of methanol,[28] formaldehyde,[31] and formic acid[27] at the surface of ice. The obtained results were in good agreement with the available experimental data.[23,26–28]

In this paper we present the results of GCMC calculations of acetone on ice at 200 K. Since understanding and modelling the adsorption of acetone on ice requires the knowledge of numerous parameters, once we determined the adsorption isotherm we characterised the adsorption properties in several ways. Thus, among others, the density profile of the adsorbed molecules along the surface normal axis, the interaction energy of the acetone molecules with the ice phase as well as with the other adsorbed molecules, and the preferred orientation of the adsorbed molecules relative to the ice phase and to the neighbouring acetone molecules are discussed in detail. The obtained results are compared to similar data obtained for the adsorption of other POH molecules, such as methanol[28] and formaldehyde,[31] in order to clarify the role played by the details of the molecular structure in the adsorption process.

2. Computational details

In order to calculate the adsorption isotherm of acetone a series of Monte Carlo simulations has been performed on the grand canonical (μ,V,T) ensemble at 200 K. The edges of the rectangular basic simulation box have been 100.0, 35.926 and 38.891 Å in the X, Y and Z directions, respectively. In the middle of the simulation box 18 molecular layers of proton-disordered I_h ice have been placed along the X direction. Each layer has been parallel to the YZ plane of the basic box, and has contained 160 water molecules. The two innermost layers of the ice crystal have been kept fixed, whereas the molecules of the outer layers have been allowed to move in the simulations. Standard periodic boundary conditions have been applied. The value of the chemical potential has been controlled through the B parameter of Adams[47]:

$$\mu = k_B T\left(B + \ln\frac{\Lambda^3}{V}\right), \quad (1)$$

where k_B is the Boltzmann constant, T is the absolute temperature, V is the volume of the system, and Λ is the thermal de Broglie wavelength of acetone:

$$\Lambda = \frac{h}{\sqrt{2\pi k_B T m}}. \quad (2)$$

In this equation m denotes the mass of the acetone molecule, and h is the Planck constant. The simulations have been performed at 28 different B values, ranging from -17 to -5, which corresponds to the chemical potentials falling in the range between -51.12 and -31.01 kJ mol^{-1}.

Although several different potential models have been proposed to describe the properties of acetone in the literature,[48–52] the majority of these models are unable to capture the mixing properties of acetone with water.[53,54] However, in the process of adsorption adsorbate–adsorbant interactions may play a very important role, in particular, at low pressures, where the adsorbate–adsorbant interaction is the main driving force of the adsorption. For this purpose, we have chosen to use the four-site KBFF acetone model of Weerasinghe and Smith,[52] which was developed to reproduce various thermodynamic properties of acetone–water mixtures. By developing this model, Weerasinghe and Smith used the three-site SPC/E water potential,[55] and therefore we also have chosen this model to describe the water molecules in our systems. The melting point of SPC/E ice is 215 K,[56,57] which is safely above the temperature of our systems of 200 K. The values of the used potential parameters are summarized in Table 1. According to these models, the total energy of the system has been assumed to be the sum of the pair interaction energies of the molecules, and the interaction of a molecule pair has been described by the sum of Lennard-Jones and charge–charge Coulomb interactions acting between their atoms.

All interactions have been truncated to zero beyond the centre–centre cut-off radius of 12.5 Å. Taking the long range part of the electrostatic interaction into account in such an inhomogeneous and anisotropic system is a non-trivial task. The application of the standard Ewald summation

Table 1 Interaction parameters of the water and acetone models used in our simulations

Molecule	Interaction site	σ/Å	ε/kJ mol^{-1}	q/e
Water	O	3.166	0.6506	−0.8476
	H	0	0	0.4238
Acetone	Me	3.748	0.8672	0.0
	C	3.360	0.3300	0.565
	O	3.100	0.5600	−0.565

technique[29,58] would lead to the simulation of an infinite stack of ice and vapour layers, whereas in using the method of reaction field correction[29,59,60] one has to face the difficulty that the system is consisted of two phases of markedly different dielectric constants. In order to adequately address this point, and investigate the importance of the exact treatment of long range electrostatics in the modelling of the adsorption process we have performed two series of simulations. In the first set we have used reaction field correction, setting the dielectric constant of the continuum beyond the cut-off sphere, ε_{RF}, to infinity (conducting boundary conditions), whereas in the second set no long range correction has been applied. This latter case corresponds to the use of the reaction field correction method with $\varepsilon_{RF} = 1$. These two sets of simulations represent the limiting cases corresponding to the lower and upper estimates of the effect of long range electrostatics in the strongly inhomogeneous system studied.

For performing the simulations we have used the MMC[61] code of Mezei. During the simulations molecule displacement and adsorbate insertion/deletion attempts have been done in an alternating order. In the particle displacement step a randomly chosen molecule has been translated to a random distance by no more than 0.25 Å, and randomly rotated around a randomly chosen space-fixed axis by the maximum angle of 15°. In an insertion/deletion attempt either, by 50% probability, a randomly chosen acetone molecule was tried to be removed from, or, by 50% probability, an extra acetone molecule was attempted to be inserted to the system. For inserting an acetone molecule the cavity-biased method of Mezei[62,63] has been used. The systems have been equilibrated by performing 10^8 Monte Carlo steps, while in the production stage 2×10^8 Monte Carlo steps have been performed for each system. In order to analyze the properties of the adsorption layer 2500 sample configurations, separated by 8×10^4 Monte Carlo steps each, have been saved in four systems, characterised by the chemical potential values of −48.54, −41.91, −40.26, and −39.43 kJ mol^{-1}, respectively.

3. Results and discussion

3.1 Adsorption isotherm

The adsorption isotherms (*i.e.*, the average number of acetone molecules $\langle N \rangle$ as a function of the acetone chemical potential μ) are shown in Fig. 1 as obtained with and without applying reaction field correction. As is seen, the two isotherms are almost identical; the only difference is that the point of condensation occurs at a slightly lower chemical potential value if no long range correction is applied. Due to the observed insensitivity of the results to the exact treatment of the long range correction of the electrostatic interaction, in the following we only present the results obtained with a choice of $\varepsilon_{RF} = 1$, unless otherwise indicated. The $\langle N \rangle$, μ and B values corresponding to the simulated points of this isotherm are numerically summarized in Table 2.

At the low μ part the obtained isotherms exhibit an exponential increase up to the μ value of about −47 kJ mol^{-1}. This part of the isotherm corresponds to the situation when the adsorption layer is far from saturation, and the adsorptions of the individual acetone molecules are independent of each other. Above this chemical potential value the slope of the isotherm starts to increasingly deviate from the exponential form, however, this slope never approaches zero. In other words, the isotherm does not exhibit any nearly

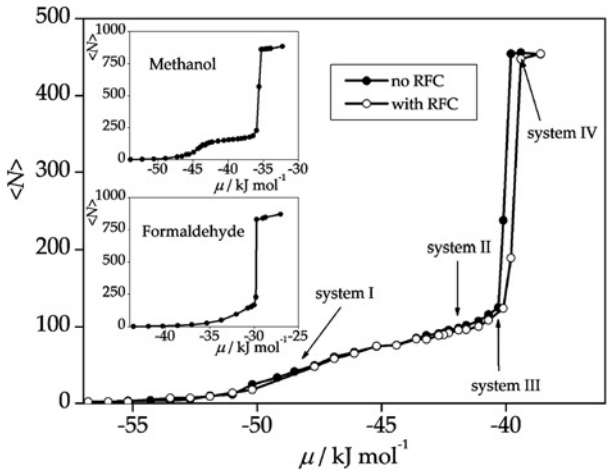

Fig. 1 Average number of acetone molecules in the basic simulation box as a function of their chemical potential. Full circles: simulations without reaction field correction, open circles: simulations applying reaction field correction under conducting boundary conditions. The lines connecting the symbols are just guides to the eye. The arrows indicate the systems that have been chosen for further analyses. The upper and lower insets show the isotherms obtained previously for methanol[28] and formaldehyde,[31] respectively.

Table 2 Data of the obtained adsorption isotherm

B	μ/kJ mol^{-1}	$\langle N \rangle$	Γ/μmol m^{-2}	p/p_0
−6.0	−38.60	453.48		
−6.5[a]	−39.43	455.65		
−6.75	−39.84	454.15		
−6.875	−40.05	237.61		
−7.00[b]	−40.26	125.05	7.46	0.882
−7.25	−40.67	115.97	6.92	0.687
−7.50	−41.09	107.26	6.40	0.535
−7.83	−41.63	101.75	6.07	0.385
−8.00[c]	−41.91	98.35	5.87	0.325
−8.21	−42.26	95.72	5.71	0.263
−8.35	−42.49	92.11	5.49	0.229
−8.50	−42.74	91.29	5.45	0.197
−8.75	−43.16	88.60	5.28	0.153
−9.00	−43.57	85.26	5.08	0.119
−9.50	−44.40	76.29	4.55	7.24×10^{-2}
−10.00	−45.23	74.20	4.43	4.39×10^{-2}
−10.50	−46.05	66.85	3.99	2.66×10^{-2}
−11.00	−46.88	60.91	3.63	1.62×10^{-2}
−11.50	−47.71	49.78	2.97	9.80×10^{-3}
−12.00[d]	−48.54	41.48	2.47	5.95×10^{-3}
−12.40	−49.20	33.63	2.01	3.99×10^{-3}
−13.00	−50.19	24.59	1.47	2.19×10^{-3}
−13.50	−51.02	11.81	0.705	1.33×10^{-3}
−14.00	−51.85	9.99	0.596	8.05×10^{-4}
−14.50	−52.68	5.41	0.323	4.88×10^{-4}
−15.00	−53.51	3.94	0.235	2.96×10^{-4}
−15.50	−54.33	3.89	0.232	1.80×10^{-4}
−16.00	−55.16	3.17	0.189	1.09×10^{-4}
−16.50	−55.99	2.39	0.142	6.61×10^{-5}
−17.00	−56.82	1.52	0.091	4.01×10^{-5}

[a] System IV. [b] System III. [c] System II. [d] System I.

constant plateau below the point of condensation at about $\mu = -40$ kJ mol^{-1}. This behaviour of the isotherm indicates that the saturated adsorption monolayer is not of a particular stability; instead the adsorption positions are continuously filled up, irrespective of whether they are at the first adsorption layer or in an outer layer. The observed shape of the isotherm is in a clear contrast with what we observed previously either for methanol or for formaldehyde. Thus, the adsorption isotherm of formaldehyde on ice shows a nearly exponential increase up to the point of condensation, indicating the Langmuir-like behaviour of this system,[31] whereas in the case of methanol the adsorption isotherm exhibits a clear plateau in a broad range of chemical potentials, indicating the remarkable stability of the adsorbed monolayer.[28] The adsorption isotherms of methanol and formaldehyde on ice, obtained in previous studies, are shown in the insets of Fig. 1 for comparison. In this respect, the features of the adsorption of acetone on ice are between those of formaldehyde and methanol. We assume that this behaviour is of energetic reason, which will be discussed in detail in the following sections.

To shed more light to the details of the adsorption process we have converted the obtained $\langle N\rangle(\mu)$ curve to the $\Gamma(p_{\mathrm{rel}})$ form, where Γ is the surface number density of the adsorbed acetone molecules, and p_{rel} is the relative pressure, *i.e.*, pressure of the vapour phase normalized by the pressure of the saturated vapour of acetone. The p_{rel} values can be calculated as[46]

$$p_{\mathrm{rel}} = \frac{p}{p_0} = \frac{\exp B}{\exp B_0}, \qquad (3)$$

where B_0 is the B value at which condensation occurs. From the $\langle N\rangle(B)$ isotherm (Table 2) we have estimated the value of B_0 to be 6.875. The value of Γ can easily be given by the expression

$$\Gamma = \frac{\langle N\rangle}{2YZ}\ , \qquad (4)$$

using the reasonable assumption that all the acetone molecules of the system are adsorbed at the surface, and taking into account the fact that, due to the applied periodic boundary conditions, the system contains two surfaces along the surface normal axis X. Since eqn (3) is only valid at the vapour phase, the $\langle N\rangle(\mu)$ isotherm can only be converted to the $\Gamma(p_{\mathrm{rel}})$ form up to the point of condensation. The obtained $\Gamma(p_{\mathrm{rel}})$ isotherm is shown in Fig. 2, and its data points are also summarised in Table 2. For comparison, the $\Gamma(p_{\mathrm{rel}})$ isotherms obtained previously for methanol[28] and formaldehyde[31] are indicated in the insets of Fig. 2.

The deviation of the obtained $\Gamma(p_{\mathrm{rel}})$ isotherm from various experimental data sets[20,23] remains in the same order as the reported deviation of the different experimental isotherms from each other. Nevertheless, the simulation underestimates the adsorption at low pressures. This is probably due to the fact that in the simulation a perfect ice surface has been used, whereas in experimental situations the surface layer of ice can be defected and can also be subject to surface melting to an unknown extent. This view is also supported by the finding of Schaff and Roberts that amorphous ice can adsorb a considerably higher amount of acetone than crystalline ice.[64,65]

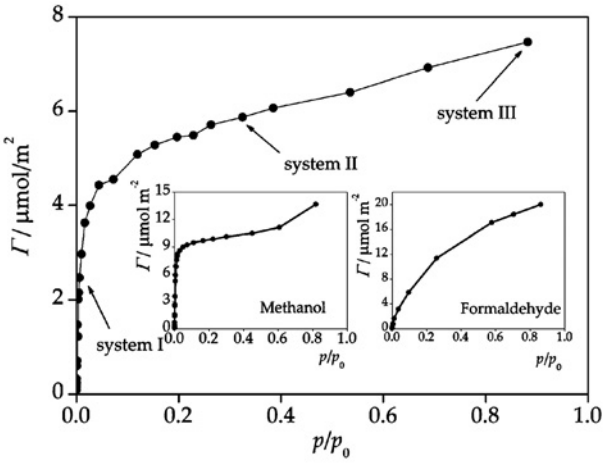

Fig. 2 Adsorption isotherm (surface density *vs*. relative pressure) of acetone on ice, as obtained from the simulations. The line connecting the symbols is just a guide to the eye. The arrows indicate the systems that have been chosen for further analyses. The left and right insets show the isotherms obtained previously for methanol[28] and formaldehyde,[31] respectively.

As is seen, the rapidly increasing part of the curve at low pressures is not followed by a saturation region; instead the isotherm exhibits a monotonous increase in the entire $0 \le p_{\mathrm{rel}} \le 1$ range, indicating the non-Langmuir nature of this adsorption. Despite this, at low pressures, *i.e.*, up to about the p_{rel} value of 0.08, the obtained $\Gamma(p_{\mathrm{rel}})$ curve can be well fitted by the Langmuir isotherm:

$$\Gamma = \Gamma_{\max}\frac{p_{\mathrm{rel}}K}{p_{\mathrm{rel}}K + 1}, \qquad (5)$$

where the parameters $\Gamma_{\max}$ and K are the saturated surface density and the partitioning coefficient between the solid and gas phase, respectively. The fitting of the obtained data in this low pressure range by the Langmuir isotherm is shown in

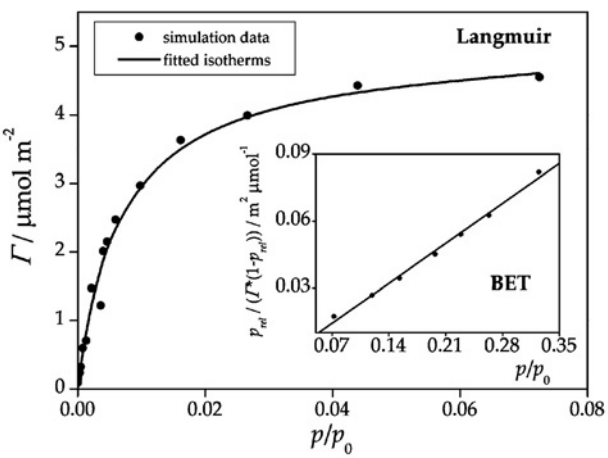

Fig. 3 Langmuir fit (solid curve) to the points of the isotherm obtained from the simulations (circles) up to the relative pressure of 0.07. The inset shows the BET fit (solid line) to these data (circles) using the linearised form of the BET equation (see eqn (7)) up to $p_{\mathrm{rel}} = 0.35$. The adjustments of the isotherms have been done in the pressure ranges shown in the figure.

Table 3 Parameters of the Langmuir and BET functions fitted to the calculated adsorption isotherm, and the monolayer capacity resulting directly from our simulations. Error bars correspond to the limits of the confidence interval of 95%

Model	Parameter	Value	Value
Langmuir	Γ_{max}	(5.04 ± 0.26) μmol m^{-2}	$(3.02 \pm 0.16) \times 10^{14}$ cm^{-2}
	K	148 ± 22	
BET	Γ_{mono}	(3.96 ± 0.34) μmol m^{-2}	$(2.38 \pm 0.20) \times 10^{14}$ cm^{-2}
	C	0.985 ± 0.16	
Simulation	Γ_{mono}	(6.52 ± 0.030) μmol m^{-2}	$(3.91 \pm 0.02) \times 10^{14}$ cm^{-2}

Fig. 3, whereas the values of Γ_{max} and K are summarised in Table 3 as resulted from this fitting.

This fact can be understood by considering the assumptions behind the Langmuir theory, namely that (i) all the adsorption sites are equivalent at the surface; (ii) the lateral interactions between the adsorbate molecules are negligible; and (iii) no multilayer adsorption occurs. Although the validity of these assumptions is difficult to be checked in experimental situations, computer simulation methods provide a unique opportunity to test them, and investigate the effect of any deviation from this ideal situation on the adsorption isotherm. In the present case, the above three assumptions are only valid up to the relative pressure value of about 0.08. As will be discussed in detail later in this paper, above this pressure the lateral interactions between the adsorbed acetone molecules become increasingly important, and further, above $p_{rel} \approx 0.5$ even multilayer adsorption occurs, as is evidenced by the increasing slope of the $\Gamma(p_{rel})$ curve above this pressure.

In order to also take the effect of this possible multilayer adsorption into account, we have performed the adjustment of the Brunauer–Emmett–Teller (BET) isotherm[66] to the simulated data points:

$$\Gamma = \frac{\Gamma_{mono} p_{rel} C}{(1 - p_{rel})[1 + p_{rel}(C - 1)]}, \qquad (6)$$

where Γ_{mono} and C are the surface density of the saturated monolayer and the BET coefficient, respectively. The BET theory differs from the Langmuir model by allowing multilayer adsorption, and hence it has to account for the interaction between consecutive adsorption layers. However, lateral interactions within a given layer are still neglected in this model. The BET parameters Γ_{mono} and C is conventionally determined by fitting the linearised form of the BET isotherm:

$$\frac{p_{rel}}{\Gamma_{mono}(1 - p_{rel})} = \frac{1}{\Gamma_{mono} C} + \frac{C - 1}{\Gamma_{mono} C} p_{rel}. \qquad (7)$$

Since the data of a BET isotherm can usually be fitted by a straight line through eqn (7) only up to the p_{rel} value of 0.35, we also limited our fitting to this pressure range. The result of this fitting is shown in the inset of Fig. 3, whereas the Γ_{mono} and C values obtained from this fitting are included in Table 3.

Although the Γ_{max} parameter of the Langmuir isotherm has basically the same physical meaning as the Γ_{mono} value of the BET isotherm (as both parameters denote the surface density of the saturated monolayer), the obtained Γ_{max} and Γ_{mono} values deviate largely, by 20–25% from each other (see Table 3). This finding again emphasizes the fact that the assumptions lying behind at least some of these functional forms are not valid for the system investigated here. This point can be checked by determining the value of Γ_{mono} directly from the simulations (as explained in detail in the following section), and be compared with the values resulted from the above fittings. Since the Γ_{mono} value of 6.52 μmol m^{-2}, resulting directly from the simulation, is about 30 and 60% larger than the values estimated from the Langmuir and BET theories, respectively (see Table 3), the invalidity of an assumption that is behind both theories can be suspected. Considering the strongly dipolar character of the acetone molecule, the invalid assumption is likely the neglect of the lateral interactions. This point will be further analysed in the following sections.

3.2 Properties of the adsorption layers

In order to characterize the structural and energetic properties of the adsorption layer in more detail, four systems, corresponding to four markedly different points of the isotherm have been chosen for further analyses. System I, characterised by the chemical potential value of -48.54 kJ mol^{-1} corresponds to the exponentially rising part of the $\langle N \rangle(\mu)$ isotherm. This chemical potential range is characterised by very low surface coverage, when the adsorbed acetone molecules are, in general, far enough from each other that their lateral interactions are negligibly small. System II, corresponding to the chemical potential value of -41.91 kJ mol^{-1} is on the slowly rising part of the isotherm. Finally, systems III and IV, being at $\mu = -40.26$ kJ mol^{-1} and $\mu = -39.43$ kJ mol^{-1}, are slightly below and slightly above the point of condensation, respectively. The points representing these systems on the isotherm are marked by arrows in Fig. 1 and 2, and are also indicated in Table 2. Equilibrium snapshot of each of the four systems are shown for illustration in Fig. 4 as taken out from the simulations.

3.2.1 Density profiles. To analyze the ordering of the acetone molecules along the surface normal axis X we have calculated the number density profiles of both the water and acetone molecules. In this calculation the positions of the molecules have been represented by that of their central atom (*i.e.* the O and C atom of water and acetone, respectively). The resulting profiles of acetone, symmetrized over the two surfaces present in the basic simulation box, are shown in Fig. 5 as obtained in systems I, II, III and IV. In addition, the density profiles of the water molecules are also shown as obtained in system I. It should be noted that the water profiles are found to be almost identical in each of the four systems analysed.

The nine peaks of water density profiles, corresponding to the nine molecular layers of the ice crystal are easily

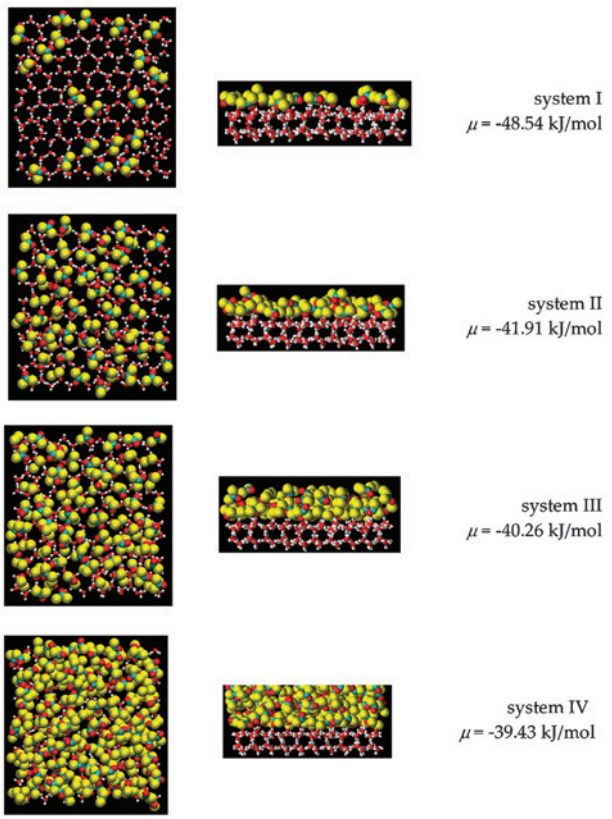

Fig. 4 Instantaneous snapshots of equilibrium configurations of the four systems chosen for detailed analyses, as picked up from the simulations. Left: top view, right: side view. The water molecules are shown by sticks only, the atoms of the acetone molecules are shown by spheres. The C, O and H atoms and methyl groups are indicated by blue, red, grey and yellow colours, respectively.

distinguishable. The water peaks are followed by the density peak of the acetone molecules that are in direct contact with

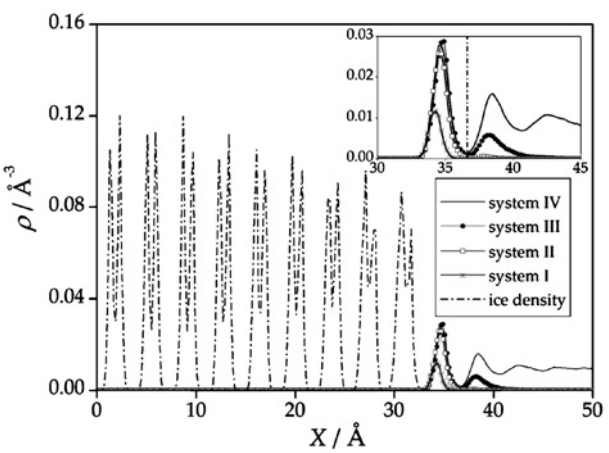

Fig. 5 Number density profiles of the acetone molecules in systems I (asterisks), II (open squares), III (filled circles), and IV (solid line). The number density profile of the water molecules in system I is also indicated (dash-dotted line). The inset shows the acetone profiles on a magnified scale. The dashed vertical line indicates the boundary of the first molecular layer of adsorbed acetone. All the profiles shown are averaged over the two surfaces that are present in the basic simulation box.

the ice surface. Clearly, this first adsorption layer is highly unsaturated in system I, where the height of this density peak is about the half of that in the other systems. In system II the adsorbed molecules form a nearly saturated monolayer at the ice surface, and traces of the second molecular layer can also be observed. It is also seen that the peak corresponding to the first layer is not only higher but also broader here than in system I, indicating that upon saturation this layer also becomes thicker. In system III the second layer is clearly building up, the surface density of acetone in this layer is already about 25% of that in the saturated first layer. Finally, system IV corresponds to condensed acetone, as the acetone density never drops to zero here. It should be noted that in this profile even the position of the fourth molecular layer can be distinguished, indicating the strong layering structure of liquid acetone at the ice surface at this low temperature.

The surface density of the saturated monolayer (*i.e.*, the monolayer capacity) can be easily calculated from the density profile, by integrating the first peak in system III or IV. (It should be noted that although in system II a few acetone molecules are already beyond the first layer, this layer is not yet completely saturated.) The resulting value of 6.516 μmol m^{-2} deviates strongly from the estimates obtained both from the Langmuir and the BET theory, as discussed in the previous section. The reasons of this deviation are discussed in detail in a following sub-section.

3.2.2 Distribution of the distances between water and acetone molecules. To characterize the structure of the first adsorption layer we have calculated the distribution of the distances of the oxygen atom of the adsorbed acetone molecules from the nearest water O and nearest water H atoms in systems I–IV. Note that here we have only taken into account the acetone molecules belonging to the first adsorption layer (*i.e.*, the carbonyl C atom of which is closer to the ice surface than the first minimum position of the acetone density profile at 36.6 Å, see Fig. 5). The obtained distributions, normalized to the average number of the adsorbed molecules in the first layer, are plotted in Fig. 6. Both of these functions are bimodal in systems II–IV, having a sharp and high peak at low distances (*i.e.*, at 2.83 and 1.80 Å in the case of O_{ac}–O_{wat} and O_{ac}–H_{wat} distributions, respectively), which is followed by a broader second peak of a much smaller height at larger distances. This second peak is, however, missing from the functions obtained in system I. Between these two peaks the distributions drop to zero, which allows us to make an unambiguous distinction between the acetone molecules that give rise to the different peaks. The positions of the first peaks correspond to the hydrogen bonding O–O and O–H distances. This means that some (in system I all) of the adsorbed acetone molecules are hydrogen bonded to the ice surface, whilst at higher surface coverage some others, being still in the first adsorption layer, are oriented away from the surface by the carbonyl group. The separate integration of the two peaks reveals that in systems II–IV 73–76 acetone molecules are hydrogen bonded to the ice surface, whereas in system II 21, and in systems III and IV 34 non-hydrogen bonded acetone molecules belong to the first adsorption layer. This finding indicates that upon saturation the acetone

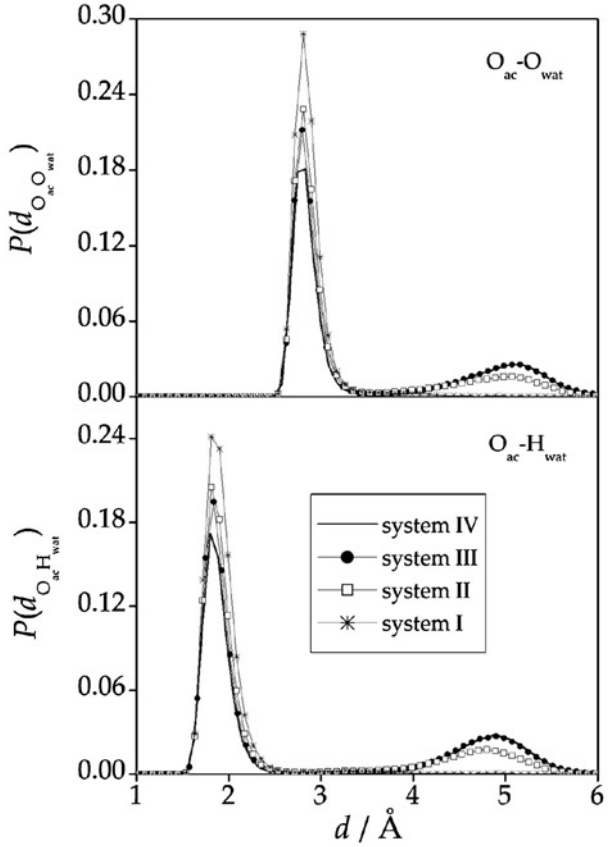

Fig. 6 Distribution of the distance of the O atom of an adsorbed acetone molecule that belongs to the first molecular layer from the nearest water O atom (top), and from the nearest water H atom (bottom). Data corresponding to systems I–IV are marked by asterisks, open squares, filled circles, and solid lines, respectively.

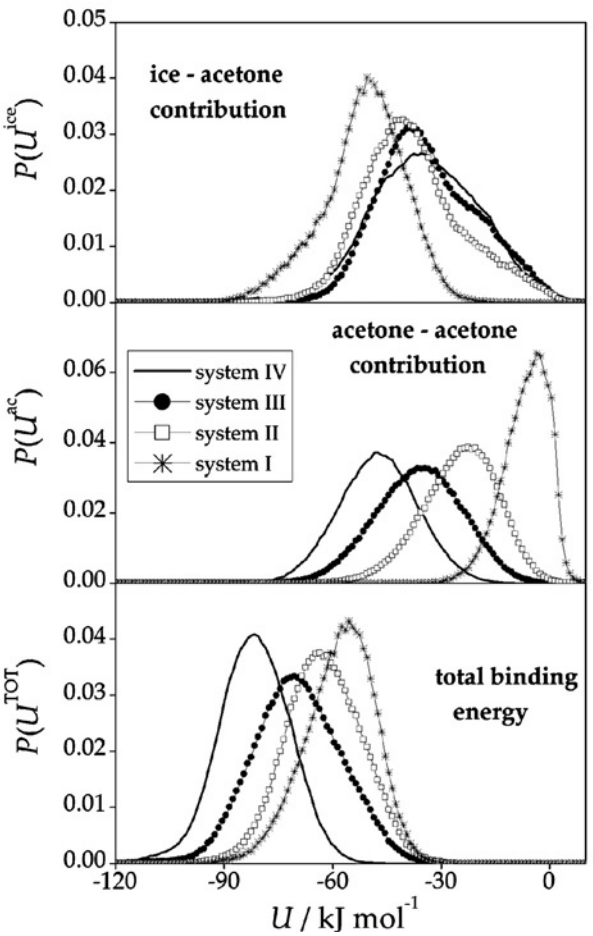

Fig. 7 Distribution of the binding energy (bottom) of the adsorbed acetone molecules (*i.e.*, the energy of their interaction with the rest of the system), as well as that of its contributions coming from the interaction with the other adsorbed molecules (middle), and with the ice phase (top). Data corresponding to systems I–IV are marked by asterisks, open squares, filled circles, and solid lines, respectively.

molecules occupy the hydrogen bonding positions first, and the non-hydrogen bonding positions start to be taken only afterwards. It is also seen that both distributions are almost identical in systems III and IV, indicating that once the first adsorption layer is completed, its structure is independent of the saturation of the outer layers.

3.2.3 Energetics of the adsorption. To analyze the energetic background of the adsorption we have calculated the binding energy of the adsorbed acetone molecules, *i.e.*, the energy of their interaction with the rest of the system U^{TOT}. In addition, the interaction energy of the individual acetone molecules has also been calculated both with the ice phase (U^{ice}) and with the other acetone molecules (U^{ac}) separately. The distributions of U^{TOT}, U^{ac} and U^{ice} are presented in Fig. 7 as obtained in the four systems analysed. As is seen, the distribution of the total binding energy is of a Gaussian shape, shifting to lower energies upon increasing the chemical potential of acetone. Thus, in system I the $P(U^{TOT})$ distribution is peaked at -55.7 kJ mol^{-1}, whereas in system IV this peak appears at -82.2 kJ mol^{-1}. This shift is due to the presence of the increasing amount of acetone molecules, and indicates that at high surface coverage the acetone–acetone interactions contribute at least as much to the thermodynamic driving force of the adsorption as acetone–ice interactions.

Not surprisingly, the evolution of the $P(U^{ac})$ distribution with the acetone chemical potential shows a rather similar picture. Thus, in system I this distribution is peaked at -3.5 kJ mol^{-1}, indicating that here the adsorbate–adsorbate interactions are still negligible. This is in clear accordance with the fact that system I is located at the exponentially rising part of the $\langle N\rangle(\mu)$ isotherm (Fig. 1), where the Langmuir theory is still applicable (see Fig. 3). The increasing amount of the acetone molecules leads evidently to the increase of the acetone–acetone interactions. Thus, in system IV (*i.e.*, in the case of condensed acetone) the peak of the $P(U^{ac})$ distribution appears at -47.7 kJ mol^{-1}. A similar binding energy value was obtained previously in liquid acetone using a different potential model.[50]

Quite a different picture is seen when the ice–acetone energy contribution is analysed. At low surface coverage (system I) the unimodal $P(U^{ice})$ distribution is peaked at -50.6 kJ mol^{-1}. This deep binding energy value suggests that here the adsorbed

Table 4 Heat of the adsorption of acetone on ice, as resulted from the present work and from previous experimental studies

T/K	$\Delta_0 H^{ads}$/kJ mol^{-1}	Method	Ref.
200	-51.4 ± 1.3	Present work	
198–223	-46 ± 7	Coated wall flow tube	23
193–223	-48.1 ± 3.1	Coated wall flow tube/Langmuir	20
	-50.3 ± 2.5	Coated wall flow tube/BET	
205–243	-54.4 ± 7.6	Chromatography	17
193–213	-55 ± 7	Volumetric	9
190–220	-49 ± 3	Coated wall flow tube/I_c ice	21
	-32 ± 6	Coated wall flow tube/I_h ice	
198–223	-52 ± 2	Chromatography	18
190–223	-43.7 ± 7.9	Coated wall flow tube	24

acetone molecules form two hydrogen bonds with the surface waters. The mean value of this distribution, resulting in -51.4 kJ mol^{-1}, can be compared to the experimental heat of the adsorption $\Delta_0 H^{ads}$, which is usually determined at very low surface coverage, when the lateral interactions are negligible, and hence $\Delta_0 H^{ads}$ does not depend on the surface coverage yet. The values of $\Delta_0 H^{ads}$ are collected in Table 4 as obtained in a number of recent experimental studies. The clear agreement between the simulated and experimental values confirms our results, and validates the choice of the used acetone potential model, which was parameterised[52] to well reproduce acetone–water interactions.

Upon increasing the acetone surface density the peak of the $P(U^{ice})$ curve gradually shifts to higher (*i.e.*, lower in magnitude) energy values, up to about -35 kJ mol^{-1}, indicating that in systems of higher surface coverage the majority of the acetone molecules form only one hydrogen bond with the ice surface. Further, these distributions exhibit two shoulders, at both sides of the main peak. The shoulder at the low energy side of the peak is located around -50 kJ mol^{-1}, *i.e.*, close to the position of the main peak of $P(U^{ice})$ in system I. This shoulder is given by the acetone molecules that are double hydrogen bonded to the ice phase. The high energy side shoulder, located at about -20 kJ mol^{-1}, clearly becomes more pronounced with increasing surface coverage. This shoulder can be attributed to the acetone molecules that do not form hydrogen bonds with the waters, yet belong to the first adsorption layer, as discussed in the previous sub-section. In order to demonstrate this, in system III we have also calculated the $P(U^{ice})$ distribution separately for the acetone molecules that give rise to the first, and for those giving rise to the second peak of $P(d_{OacOwat})$ (see Fig. 8). As is seen, these two types of adsorbed acetone molecules correspond to completely different $P(U^{ice})$ distributions. The peak of the hydrogen bonded acetones appears at about the same position than the peak of $P(U^{ice})$ in system III (*i.e.*, at -40.3 kJ mol^{-1}), whereas that of the non-hydrogen bonded acetones is at -18.7 kJ mol^{-1}, where the shoulder of the full distribution is located. This relatively strong interaction of the non-hydrogen bonded acetone molecules with ice is probably due to the electrostatic interaction of the large dipole moment of the acetone molecule with the charge distribution of the ice phase.

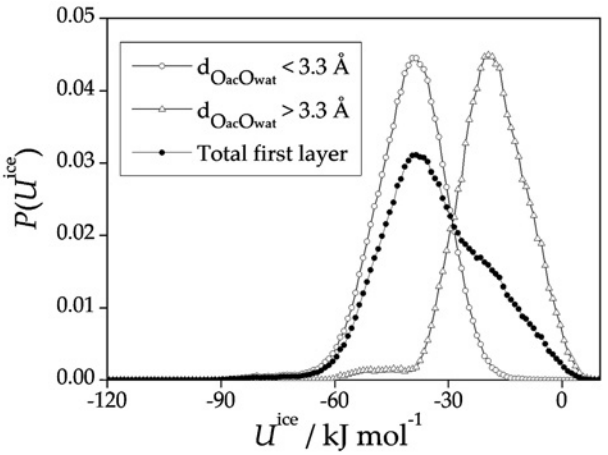

Fig. 8 Distribution of the interaction energy of an adsorbed acetone molecule of the first molecular layer with the ice phase in system III, considering only those molecules the O atom of which is closer to the nearest water O atom than 3.3 Å (open circles), only those molecules the O atom of which is farther from the nearest water O atom than 3.3 Å (open triangles), and all the molecules of the first molecular layer (full circles).

3.2.4 Orientation of adsorbed molecules. The orientation of a rigid body relative to an external direction (and, hence, also relative to an external plane) can be fully described by two independent orientational variables. Therefore, the orientational statistics of molecules relative to a flat surface can only be given unambiguously by the bivariate joint distribution of two such variables.[67,68] We have previously demonstrated that the polar angles ϑ and ϕ of the surface normal vector in a local Cartesian frame fixed to the individual molecules represent a suitable choice of these variables.[67,68] In the present study this local frame has been defined in the

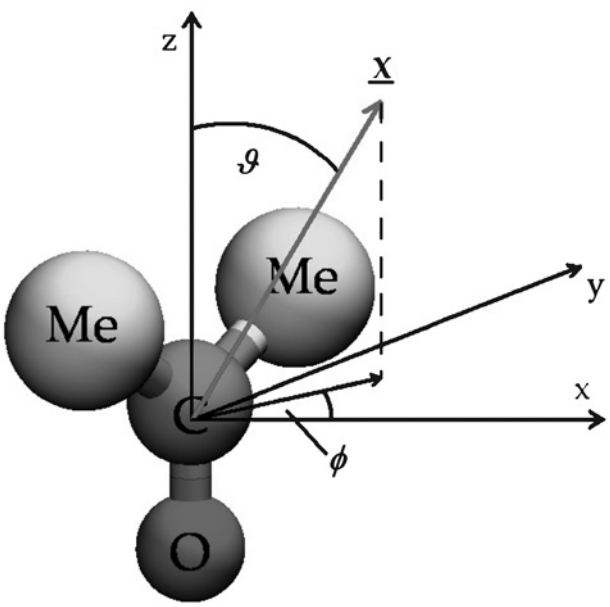

Fig. 9 Definition of the local Cartesian frame fixed to the individual acetone molecules, and of the polar angles ϑ and ϕ describing the orientation of the surface normal vector, $\underline{X}$, pointing away from the ice phase, in this frame.

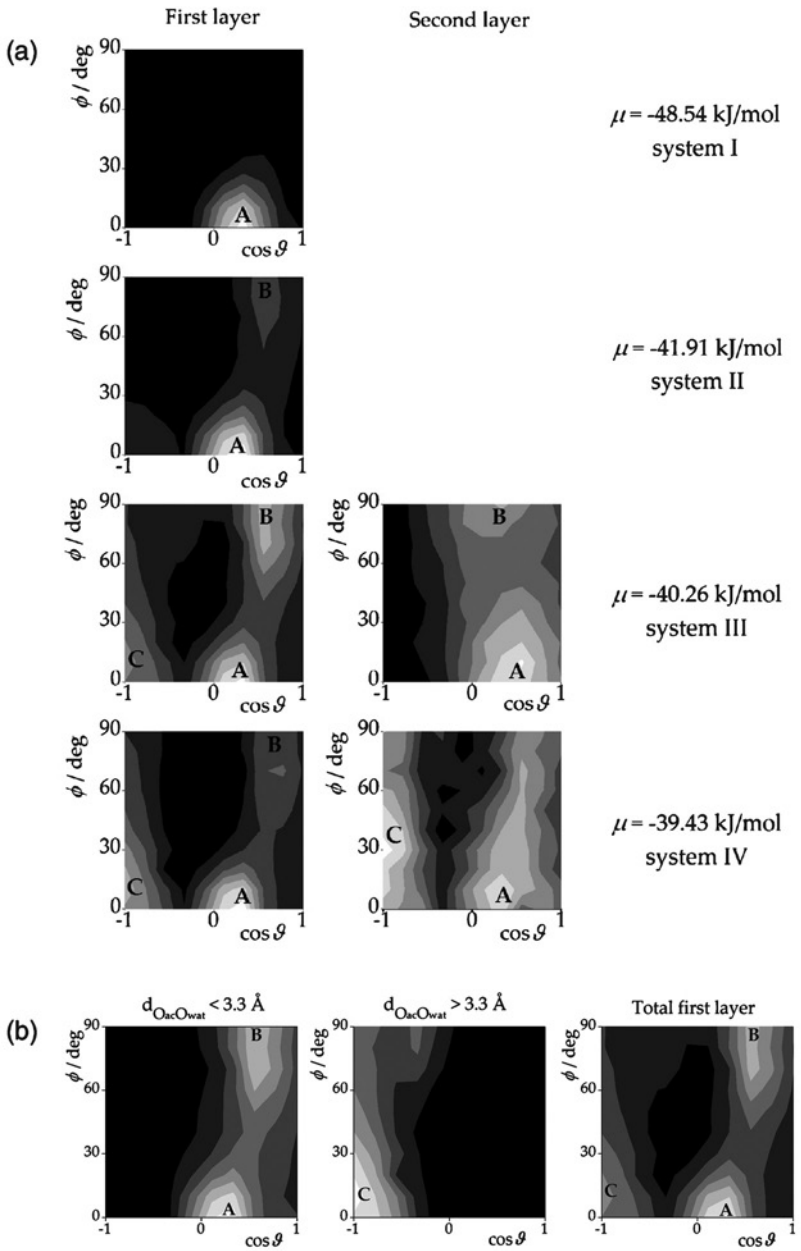

Fig. 10 (a) Orientational maps of the adsorbed acetone molecules belonging to the first (left column) and second (right column) molecular layer relative to the ice surface in systems I–IV (from the top to the bottom). (b) Orientational map of the acetone molecules of the first layer in system III the O atom of which is closer to the nearest water O atom than 3.3 Å (left), the O atom of which is farther from the nearest water O atom than 3.3 Å (middle), and all the first layer acetone molecules (right). The peaks corresponding to the different preferred acetone orientations are marked with A–C. Lighter shades of grey indicate higher probabilities.

following way. The origin is located at the carbonyl C atom; the z axis lies along the dipole vector of the acetone molecule pointing from the O to the C atom of the carbonyl group, x is the molecular normal axis, and the y axis is perpendicular of the above two axes. Thus, ϑ is the angle between the interface normal vector pointing away from the ice phase $\underline{X}$ and the molecular dipole vector, and ϕ is the angle between the molecular normal vector and the projection of $\underline{X}$ to the plane perpendicular to the main symmetry axis of the molecule. The definition of this local Cartesian frame and of the polar angles ϑ and ϕ is demonstrated in Fig. 9. It should be noted that while the direction of the z axis of the molecule-fixed frame is set by the geometry of the acetone molecule, and hence ϑ can take any value between 0 and 180°, the molecule normal axis x can equally be directed to two opposite directions. The direction of this axis is always chosen in such a way that the relation $\phi \leq 90^\circ$ holds. It should also be noted that ϑ is the angle of two general spatial vectors, but ϕ is formed by two vectors restricted to lie in a given plane by definition, and hence uncorrelated orientation of the molecules with the surface results in a uniform bivariate distribution only if cos ϑ and ϕ are chosen as independent variables.

The bivariate $P(\cos\vartheta,\phi)$ orientational distributions of the adsorbed molecules are plotted in Fig. 10a as obtained in the first and second molecular layers of the four systems studied, using different tones to represent the different values of the functions. In system I, *i.e.*, at low surface coverage the acetone molecules have only one preferred orientation, which is denoted here by A. This orientation is characterised by the cos ϑ and ϕ values of 0.3 and 0°, respectively. In this orientation, the acetone molecule is slightly tilted, pointing to the ice surface by the O atom, the two methyl groups being at equal distance from the ice surface. At higher surface coverage (system II) another orientation, corresponding to $\cos\vartheta = 0.55$ and $\phi = 90°$ also becomes preferred. In this orientation, marked with B, the main symmetry axis of the molecule is only slightly more tilted than in orientation A, but the molecular plane is now perpendicular to the ice surface. Finally, in systems III and IV, *i.e.*, when the first molecular layer is followed by a second one, and hence the acetone molecules belonging to the first layer have acetone neighbours also in the second layer, the preference of a third orientation, corresponding to the cos ϑ value of -1 emerges. In this orientation, denoted here by C, the acetone molecule is perpendicular to the ice surface, pointing by its O atom away from the ice phase. It is also seen that in the second layer of system III, where this layer is the outmost one, the molecules only prefer orientations A and B, without any sign of the preference of orientation C. It should be noted that very similar orientational preferences have been observed at the surface of liquid acetone.[69] On the other hand, in system IV, where the second layer is followed by other layers of acetone, orientation C is also clearly preferred in the second layer. The orientations A, B and C, preferred by the acetone molecules in the different systems are illustrated in Fig. 11.

The physical background of these orientational preferences can be understood by considering the orientations of the water molecules at the surface layer of the ice phase. The four possible orientations of these molecules, denoted by 1–4 here are also shown in Fig. 11. In two of these orientations

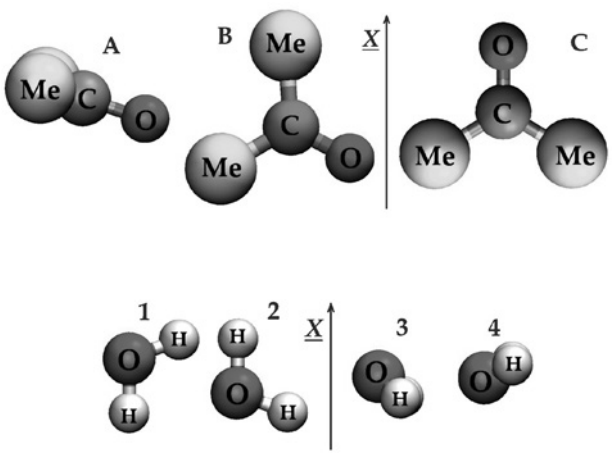

Fig. 11 Illustration of the preferred orientations of the acetone molecules adsorbed at the ice surface (top row) and surface water molecules (bottom row) relative to the ice surface. $\underline{X}$ is the surface normal vector, pointing away from the ice phase.

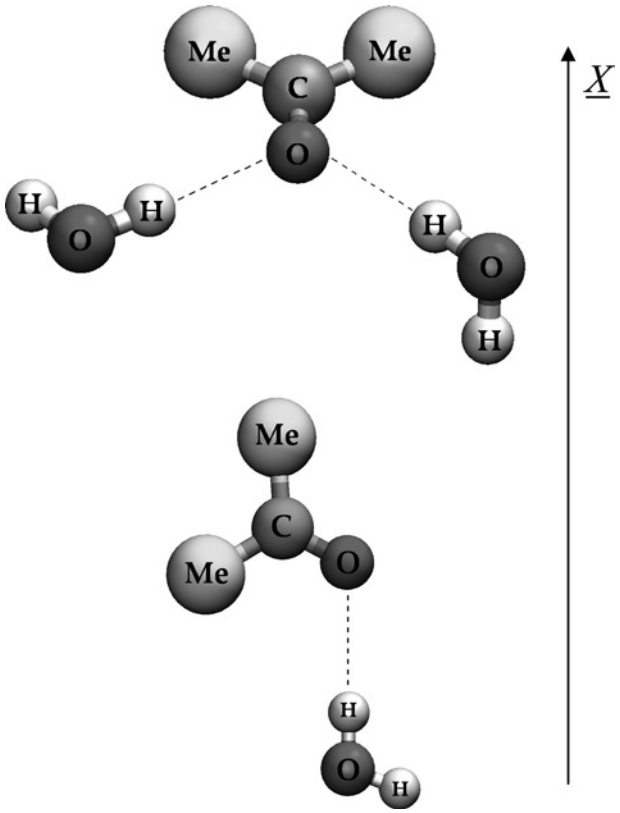

Fig. 12 Possible hydrogen bonding patterns between the adsorbed acetone molecules of the first molecular layer and surface water molecules of the ice phase in their preferred orientations. $\underline{X}$ is the surface normal vector, pointing away from the ice phase.

(*i.e.*, 1 and 4) the water molecule points flatly to the vapour phase by one or two of its O–H bonds, whereas in orientation 2 one of the O–H bonds sticks straight to the vapour phase. Thus, an adsorbed acetone molecule of orientation A can form two hydrogen bonds with the surface waters of either orientation 1 or 4, whereas in orientation B an acetone molecule can accept one hydrogen bond from a surface water of orientation 2. These possible hydrogen bonding patterns between the adsorbed acetone and surface water molecules are illustrated in Fig. 12.

It should be noted that the acetone molecules of orientations A and B can be related to the β-acetone, and those of orientation C to the α-acetone molecules of Schaff and Roberts,[65] who made this distinction by studying the desorption of acetone from the ice surface by Fourier transform infrared reflection–absorption (FTIR-RA) spectroscopy. Similar distinction was made by Mitlin and Leung between "dangling acetone–OH complexes" (*i.e.*, acetones H-bonded to ice, orientations A and B) and "van der Waals complexes" (*i.e.*, acetones in orientation C) by FTIR-RA spectroscopic measurements.[70] Orientation A was also observed by Marinelli and Allouche at defected ice surface by *ab initio* calculations.[71] Further, orientations analogous to A and B were also observed in the adsorption layer of formaldehyde on ice, although with considerably smaller adsorption energies.[31] This difference of the adsorption energies of formaldehyde and acetone, seen also in experimental studies,[23]

and also the lack of the preference for alignment C of formaldehyde can be explained by the positive inductive effect of the methyl groups of acetone, which results in a considerably larger dipole moment than that of formaldehyde.

In the light of the observed orientational preferences we can now interpret the results of the previous analyses. The appearance of the various preferred orientations with increasing chemical potential is in clear accordance with the evolution of the distribution of the binding energy and its contributions from the ice phase and from the other acetone molecules (see Fig. 7). Thus, in system I, at low surface coverage, the adsorbed molecules are in orientation A, and form two hydrogen bonds with the ice phase. Up to the completion of the adsorption sites where acetone molecules can be bound in this orientation (*i.e.*, up to the p_{rel} value of about 0.07) the adsorption isotherm exhibits Langmuir behaviour. This is not surprising, since in this pressure range the assumptions behind the Langmuir theory (*i.e.*, all the adsorption sites are equivalent, and lateral interactions are negligible) are valid. In the light of this finding, we can now interpret the Γ_{max} value, obtained from the Langmuir fit of the isotherm at low pressures (eqn (5)) as the saturation surface density of the adsorption sites to which an acetone molecule of orientation A can be bound. These adsorption sites require the presence of two nearby surface water molecules, either both in orientation 1, or both in orientation 4, or one in orientation 1 and the other one in orientation 4. The value of Γ_{max} is 5.04 μmol m^{-2} (see Table 3), which is in good agreement with the experimental value of 4.5 ± 1.2 μmol m^{-2}.[23] However, this value is about 30% smaller than the surface density of the saturated first adsorption layer of 6.52 μmol m^{-2}, as obtained from the integration of the first peak of the acetone density profile (see Fig. 5). Contrary to Γ_{max}, this latter value corresponds to the saturation surface density of the entire first adsorption layer, including the acetone molecules of orientations B and C, as well. This result also suggests that the experimental value of the saturated surface density, derived from the Langmuir fit of the low pressure data,[23] probably reflects again the surface density solely of these strongly bound (*i.e.*, double hydrogen bonded) acetone molecules.

Furthermore, the second peak of the $P(d_{OacOwat})$ and $P(d_{OacHwat})$ distributions (see Fig. 6) can be clearly attributed to the acetone molecules of orientation C. To demonstrate this, we have calculated the $P(\cos\vartheta,\phi)$ orientational map separately for those acetone molecules that give rise to the first, and for those that give rise to the second peak of $P(d_{OacOwat})$ in the first layer of system III. These maps, shown in Fig. 10b, clearly indicates that the molecules that give rise to the second peak of $P(d_{OacOwat})$ (and hence to the peak of $P(U^{ice})$ at about −18 kJ mol^{-1}, see Fig. 8) are in orientation C, whereas the other molecules are either in orientation A or B. The fact that the first adsorption layer is only completed after the second layer started to be building up, seen from the analysis of the acetone density profiles (Fig. 5) can also be understood now. Molecules in orientation C only appear in the first layer when it is not the outmost one, *i.e.*, when at least traces of the second layer are also present in the system.

In the first layer, orientations A and B are stabilised by the possible hydrogen bonds the molecules can form with the surface waters. On the other hand, in the outmost layer these orientations are preferred because of the same reasons as at the surface of liquid acetone.[69] These orientations are further stabilised by the possibility of forming head-to-tail dipole–dipole pairs with the molecules of the same orientation in the next layer. Finally, orientation C is stabilised by the dipole–dipole interaction with the roughly oppositely aligned molecules of orientations A and B of the outer molecular layer.

4. Summary and conclusions

In this paper we presented a detailed investigation of the adsorption process of acetone at the surface of I_h ice by means of computer simulation. In the analysis we exploited the full potential of the grand canonical Monte Carlo method. Thus, by systematically varying the chemical potential of the adsorbate, we could simulate a complete adsorption experiment, and, at the same time, the simulated configurations provided a molecular level insight into the properties of the adsorption layer at various stages of the adsorption process (*i.e.*, at various surface coverages). We reproduced well the experimental heat of adsorption, which gives us confidence in the adequacy of the potential models used, and thus in the result of the simulations.

The obtained isotherm exhibits a Langmuir-like behaviour only at rather low pressures, up to the relative pressure of about 0.07. In this pressure range the assumptions that are behind the Langmuir theory are valid. The acetone molecules are adsorbed at the surface in a given orientation (orientation A, Fig. 11), forming two hydrogen bonds with the surface waters, while their interaction with each other is negligible. The surface density of the adsorption sites at which the acetone molecules can be bound in this way is estimated to be 5.04 μmol m^{-2} from the Langmuir fit of the calculated isotherm at low pressures.

Once these adsorption sites are saturated, new molecules can only be attached to other type of sites of the surface, where they have to adopt a different orientation. In this orientation (orientation B, Fig. 11) the adsorbed acetone molecule can form only one hydrogen bond with the dangling O–H group of a surface water molecule. Since these two orientations of the adsorbed acetone molecules, the preference of which is dictated by the possibility of forming hydrogen bonds with the surface waters, are the same as what are preferred at the surface of liquid acetone,[69] these orientations are not only preferred in the first, but also in the outmost molecular layer. The dipolar orientation of these molecules then gives rise to the appearance of a third orientation, preferred only in the inner layers of acetone (orientation C, Fig. 11). Thus, molecules of this orientation appear in the first molecular layer only after the second layer has started to be building up. The surface density of the fully saturated first molecular layer, containing molecules in all three of these preferred orientations is calculated to be 6.52 μmol m^{-2}.

Acknowledgements

This work has been supported by the Hungarian–French Intergovernmental Science and Technology Program (BALATON) under project No. FR-18/2007, and by the Hungarian OTKA Foundation under Project No. T049673. P.J. is a Bolyai János fellow of the Hungarian Ministry of Education, which is gratefully acknowledged. The authors are grateful to Albert P. Bartók (Cavendish Laboratory, Cambridge) for providing the coordinates for the I_h ice crystal.

References

1 H. B. Singh, M. Kanadikou, P. J. Crutzen and D. J. Jacob, *Nature*, 1995, **378**, 50.
2 C. Wang, P. J. Crutzen, V. Ramanathan and S. F. William, *J. Geophys. Res.*, 1995, **100**, 11509–11516.
3 D. M. Winkler and C. E. Trepte, *Geophys. Res. Lett.*, 1998, **25**, 3351.
4 M. Molina, *Oceanus*, 1988, **31**, 47.
5 S. Solomon, S. Borrmann, R. R. Garcia, R. Portmann, L. Thomason, L. R. Poole, D. Winkler and M. P. McCormick, *J. Geophys. Res.*, 1997, **102**, 21411.
6 M. A. Zondlo, P. K. Hudson, A. J. Prenni and M. A. Tolbert, *Annu. Rev. Phys. Chem.*, 2000, **51**, 473.
7 A. J. Heymsfield and R. M. Sabin, *J. Atmos. Sci.*, 1989, **46**, 2252.
8 M. G. Lawrence and P. J. Crutzen, *Tellus*, 1998, **50B**, 2639.
9 F. Domine and L. Rey-Hanot, *Geophys. Res. Lett.*, 2002, **29**, 1873.
10 W. Cantrell and A. Heymsfield, *Bull. Am. Meteor. Soc.*, 2005, **86**, 795.
11 H. R. Pruppacher and J. D. Klett, *Microphysics of Clouds and Precipitation*, Reidel, Dordrecht, 1997.
12 M. Riikonen, M. Sillanpaa, L. Virta, D. Sullivan, J. Moilanen and I. Luukkonen, *Appl. Opt.*, 2000, **39**, 6080.
13 J. Goodman, O. B. Toon, R. F. Pueschel, K. G. Snetsinger and S. J. Verma, *J. Geophys. Res.*, 1989, **94**, 16449.
14 H. Singh, Y. Chen, A. Tabazadeh, Y. Fukui, I. Bey, R. Yantosca, D. Jacob, F. Arnold, K. Wohlfrom, E. Atlas, F. Flocke, D. Blake, B. Heikes, J. Snow, R. Talbot, G. Gregory, G. Sachse, S. Vay and Y. Kondo, *J. Geophys. Res.*, 2000, **105**, 3795.
15 D. J. Jacob, B. D. Field, E. M. Jin, I. Bey, Q. Li, J. A. Logan, R. M. Yantosca and H. P. Singh, *J. Geophys. Res.*, 2002, **107**, 4100.
16 T. L. Couch, A. L. Sumner, T. M. Dassau, P. B. Shepson and R. E. Honrath, *Geophys. Res. Lett.*, 2000, **27**, 2241.
17 C. Guimbaud, A. Grannas, P. Shepson, J. Fuentes, H. Boudries, J. Botten-Heim, F. Domine, S. Houdier, S. Perrier, T. Biesenthal and B. Splawn, *Atmos. Environ.*, 2002, **36**, 2743.
18 T. Bartels-Rausch, C. Guimbaud, H. W. Gäggeler and M. Ammann, *Geophys. Res. Lett.*, 2004, **31**, L16110.
19 P. K. Hudson, M. A. Zondlo and M. A. Tolbert, *J. Phys. Chem. A*, 2002, **106**, 2882.
20 N. Peybernès, C. Marchand, S. Le Calvé and P. Mirabel, *Phys. Chem. Chem. Phys.*, 2004, **6**, 1277.
21 P. Behr, A. Terziyski and R. Zellner, *J. Phys. Chem. A*, 2006, **110**, 8098–8107.
22 D. J. Donaldson and D. Anderson, *J. Phys. Chem. A*, 1999, **103**, 871–876.
23 A. K. Winkler, N. S. Holmes and J. N. Crowley, *Phys. Chem. Chem. Phys.*, 2002, **4**, 5270.
24 P. Behr, U. Scharfenort, A. Terziyski, K. Demiral and R. Zellner, in *Combustion and Atmospheric Pollution, International Symposium on Atmospheric Pollution*, ed. G. D. Ray, S. M. Forlov and A. M. Starik, Torus Press, Moscow, 2003, pp. 575–578.
25 O. Sokolov and J. P. D. Abbatt, *J. Phys. Chem. A*, 2002, **106**, 775.
26 P. von Hessberg, N. Pouvesle, A. K. Winkler, G. Schuster and J. N. Crowley, *Phys. Chem. Chem. Phys.*, 2008, **10**, 2345.
27 P. Jedlovszky, G. Hantal, K. Neuróhr, S. Picaud, P. N. M. Hoang, P. von Hessberg and J. N. Crowley, *J. Phys. Chem. C*, 2008, **112**, 8976.
28 P. Jedlovszky, L. Pártay, P. N. M. Hoang, S. Picaud, P. von Hessberg and J. N. Crowley, *J. Am. Chem. Soc.*, 2006, **128**, 15300.
29 M. P. Allen and D. J. Tildesley, *Computer Simulation of Liquids*, Clarendon Press, Oxford, 1987.
30 B. Collignon and S. Picaud, *Chem. Phys. Lett.*, 2004, **393**, 457.
31 G. Hantal, P. Jedlovszky, P. N. M. Hoang and S. Picaud, *J. Phys. Chem. C*, 2007, **111**, 14170.
32 N. Peybernès, S. Le Calvé, P. Mirabel, S. Picaud and P. N. M. Hoang, *J. Chem. Phys. B*, 2004, **108**, 17425.
33 S. Picaud, P. N. M. Hoang, N. Peybernès, S. Le Calvé and P. J. Mirabel, *J. Chem. Phys.*, 2005, **122**, 194707.
34 S. Picaud and P. N. M. Hoang, *J. Chem. Phys.*, 2000, **112**, 9898.
35 V. Ballenegger, S. Picaud and C. Toubin, *Chem. Phys. Lett.*, 2006, **432**, 78.
36 E. A. Muller, L. F. Rull, L. F. Vega and K. E. Gubbins, *J. Phys. Chem.*, 1996, **100**, 1189.
37 E. A. Muller and K. E. Gubbins, *Carbon*, 1998, **36**, 1433.
38 E. A. Muller, F. R. Hung and K. E. Gubbins, *Langmuir*, 2000, **16**, 5418.
39 J. K. Brennan, T. J. Bandosz, K. T. Thomson and K. E. Gubbins, *Coll. Surf. A*, 2001, **187–188**, 539.
40 A. Stirolo, A. A. Chialvo, K. E. Gubbins and P. T. Cummings, *J. Chem. Phys.*, 2005, **122**, 234712.
41 F. Moulin, S. Picaud, P. N. M. Hoang, L. Pártay and P. Jedlovszky, *Mol. Simul.*, 2006, **32**, 487.
42 F. Moulin, S. Picaud, P. N. M. Hoang and P. Jedlovszky, *J. Chem. Phys.*, 2007, **127**, 164719.
43 G. Garberoglio, *Langmuir*, 2007, **23**, 12154.
44 J. Puibasset and R. J. M. Pellenq, *J. Chem. Phys.*, 2003, **118**, 5613.
45 J. Puibasset and R. J. M. Pellenq, *J. Chem. Phys.*, 2005, **122**, 094704.
46 C. D. Daub, G. N. Patey, D. B. Jack and A. K. Sallabi, *J. Chem. Phys.*, 2006, **124**, 114706.
47 D. J. Adams, *Mol. Phys.*, 1975, **29**, 307.
48 M. Ferrario, M. Haughney, I. R. McDonald and M. L. Klein, *J. Chem. Phys.*, 1990, **93**, 5156.
49 W. L. Jorgensen, J. M. Briggs and M. L. Contreras, *J. Phys. Chem.*, 1990, **94**, 1683.
50 P. Jedlovszky and G. Pálinkás, *Mol. Phys.*, 1995, **84**, 217.
51 J. M. Hermida-Ramón and M. A. Ríos, *J. Phys. Chem. A*, 1998, **102**, 2594.
52 S. Weerasinghe and P. E. Smith, *J. Chem. Phys.*, 2003, **118**, 10663.
53 A. Perera and F. Sokolic, *J. Chem. Phys.*, 2004, **121**, 11272.
54 A. Perera, F. Sokolic, L. Almásy, P. Westh and Y. Koga, *J. Chem. Phys.*, 2005, **123**, 024503.
55 H. J. C. Berendsen, J. R. Grigera and T. P. Straatsma, *J. Phys. Chem.*, 1987, **91**, 6269.
56 C. Vega and J. L. F. Abascal, *J. Chem. Phys.*, 2005, **123**, 144504.
57 R. G. Fernández, J. L. F. Abascal and C. Vega, *J. Chem. Phys.*, 2006, **124**, 144506.
58 P. P. Ewald, *Ann. Phys.*, 1921, **21**, 1087.
59 J. A. Barker and R. O. Watts, *Mol. Phys.*, 1973, **26**, 789.
60 M. Neumann, *J. Chem. Phys.*, 1985, **82**, 5663.
61 M. Mezei, *MMC: Monte Carlo program for simulation of molecular assemblies*, URL: http://inka.mssm.edu/~mezei/mmc.
62 M. Mezei, *Mol. Phys.*, 1980, **40**, 901.
63 M. Mezei, *Mol. Phys.*, 1987, **61**, 565. Erratum: *ibid.* 1989, **67**, 1207.
64 J. E. Schaff and J. T. Roberts, *J. Phys. Chem.*, 1996, **100**, 14151.
65 J. E. Schaff and J. T. Roberts, *Langmuir*, 1998, **14**, 1478.
66 S. Brunauer, P. H. Emmett and E. Teller, *J. Am. Chem. Soc.*, 1938, **60**, 309.
67 P. Jedlovszky, Á. Vincze and G. Horvai, *J. Chem. Phys.*, 2002, **117**, 2271.
68 P. Jedlovszky, Á. Vincze and G. Horvai, *Phys. Chem. Chem. Phys.*, 2004, **6**, 1874.
69 L. Pártay, P. Jedlovszky and G. Horvai, *J. Phys. Chem. B*, 2005, **109**, 12014.
70 S. Mitlin and K. T. Leung, *Surf. Sci.*, 2002, **505**, L227.
71 F. Marinelli and A. Allouche, *Chem. Phys.*, 2001, **272**, 137.